Solar Fuels Engineering Lab at Columbia University

PI: Daniel V. Esposito, Dept. of Chemical Engineering, Columbia Electrochemical Energy Center (CEEC)

solarfuelsengineering.com
@espo_lab on twitter

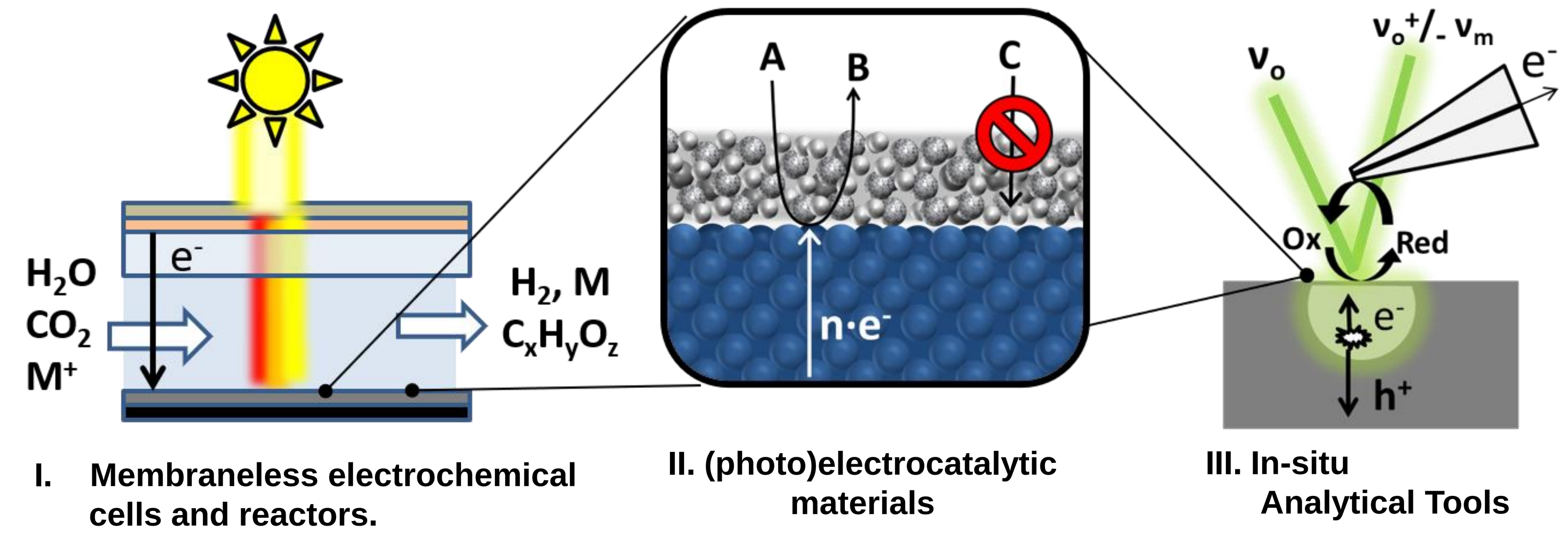

I. Membraneless electrochemical cells and reactors.
II. (photo)electrocatalytic materials
III. In-situ Analytical Tools

Membraneless Electrochemical Cells

Motivation: Electrolyzer capital costs must be decreased in a renewable energy future where electrolyzers are only operated for 20-30% of the day.

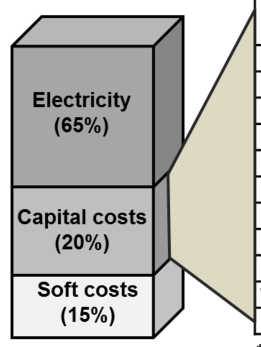

Component	% of System cost
Bipolar plates*	20.9%
Current collectors*	7.0%
MEA manufacture*	4.1%
Membranes*	2.1%
Anode catalyst*	2.5%
Cathode catalyst*	0.8%
Other stack*	3.7%
Power electronics	20.0%
H2 management	10.0%
Water delivery system	6.0%
Balance of system	23.0%

*PEM Electrolyzer stack components

Breakdown of capital costs for a typical PEM electrolysis system. Data from Bertuccioli, L., et al. "Study on development of water electrolysis in the EU", Study Dev. Water Electrolysis EU, by E4tech S'arl with Elem. Energy Ltd Fuel Cells Hydrog. Joint Undertaking (2014), 1–160.

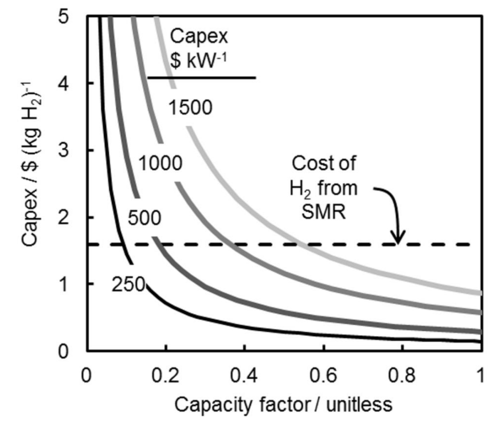

Capital expenditures (capex) of an electrolyzer system normalized to the total amount of H$_2$ generated over a 10 year lifetime while operating at 1.5 A cm^{-2} and an electrolysis efficiency of 78 %.[1]

Flow-induced Product Separation[2-4]

Key idea: use fluid flow to separate electrolysis products from flow-through electrodes.

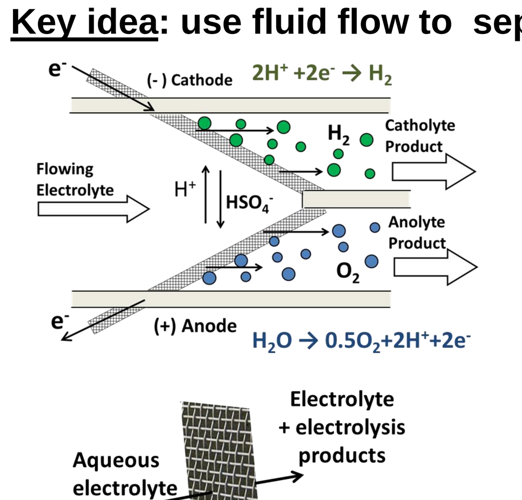

Top: Schematic top view of membraneless electrolyzer with angled mesh electrodes. **Bottom:** mesh flow-through electrode.

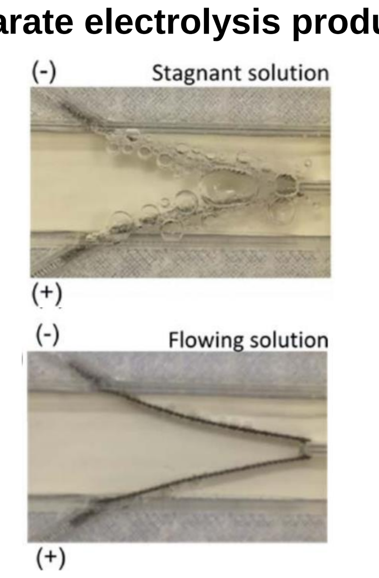

Images of bubble evolution during electrolyzer operation under stagnant and flowing conditions in 0.5 M H$_2$SO$_4$.

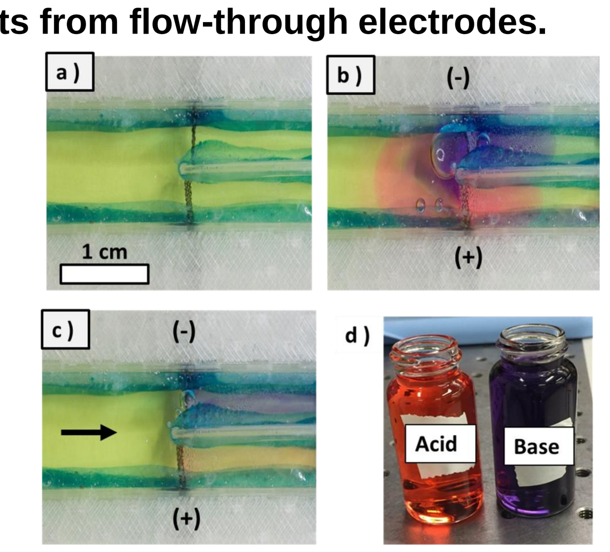

Visualizing local pH in 1 M KNO3 and a universal pH indicator dye during a) J= 0.0 mA cm^{-2}), (b) J= 62.5 mA cm^{-2} in stagnant electrolyte, and (c) J= 62.5 mA cm^{-2} with flow rate = 0.41 mL s^{-1}. (d) Acid and base collected during operation shown in (c).

Buoyancy-induced Product Separation[5]

Key Idea: Selective placement of electrocatalyst allows operation without pumping.

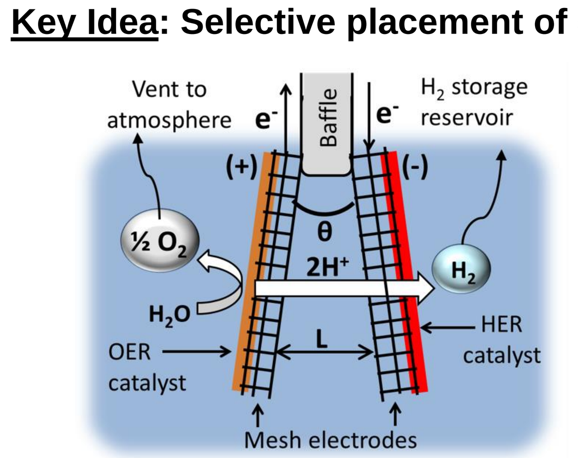

Schematic side-view of "asymmetric" electrodes with catalyst deposited on outer surfaces.

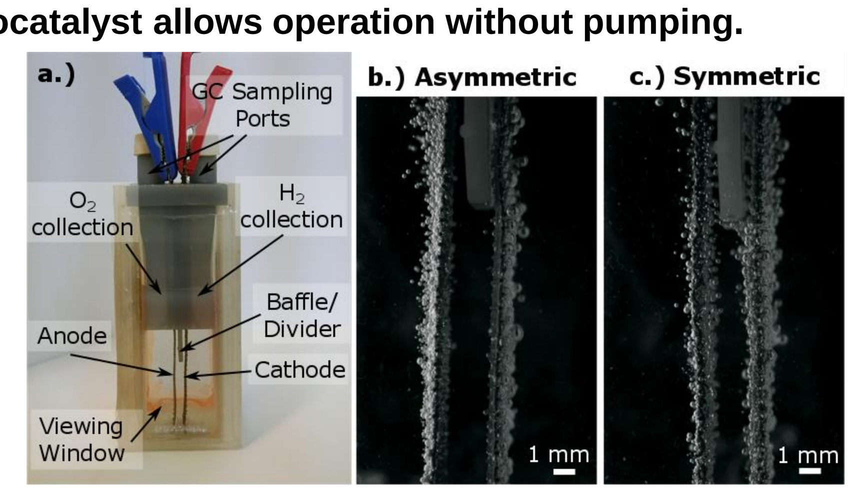

a.) 3D printed test cell for evaluating mesh electrode performance. b.), c.) Side-view snap shot images of of mesh electrodes during electrolysis in 0.5 M H$_2$SO$_4$ at 150 mA cm^{-2}.

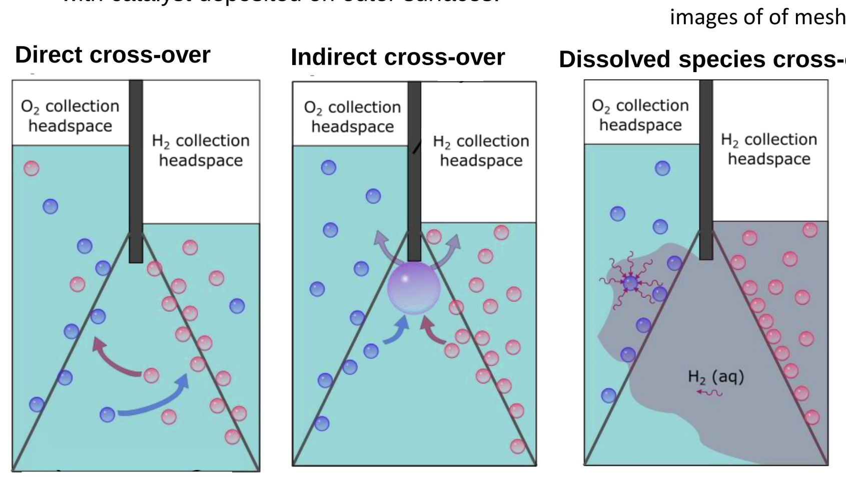

Mechanisms of product crossover in passive membraneless electrolyzers.

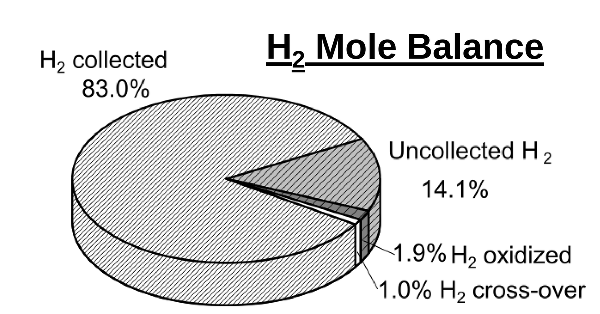

Mole balance on H$_2$ generated during electrolysis with asymmetric electrodes operated with an electrode angle of 30° and a constant current density of 40 mA cm^{-2} for 3.9 minutes.

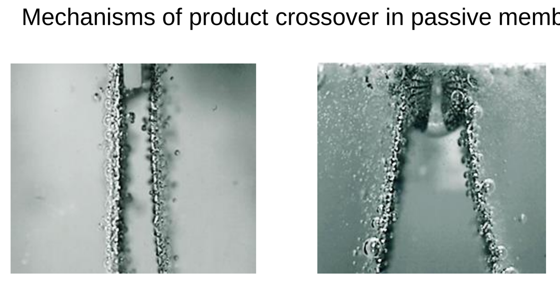

High speed video still frames showing direct and indirect cross-over and events

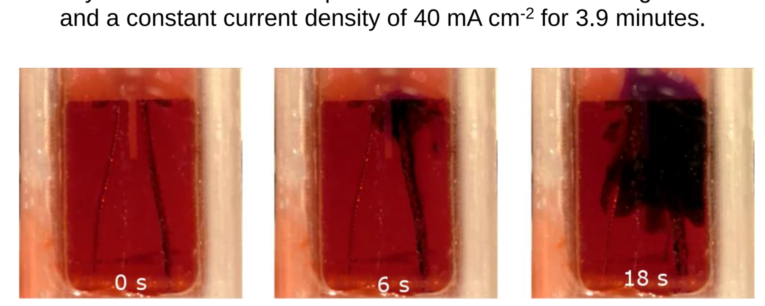

Left: pH indicator dye experiment for water electrolysis at an applied current of 40 mA cm^{-2} in a neutral salt electrolyt illustrating dissolved species cross-over.

Publications

[1] D. V. Esposito, Joule, 1(4), 651-658, 2017.
[2] G. D. O'Neil, C. D. Christian, D. E. Brown, D. V. Esposito, J. Electrochem Soc, 163(11), F3012-F3019, 2016.
[3] J. T. Davis, D. V. Esposito, J. Phys. D., 50(8), 084002, 2017.
[4] O. O. Talabi, A. E. Dorfi, G. D. O'Neil, D. V. Esposito, Chem Commun, 53(57), 8006-8009, 2017.
[5] J. T. Davis, J. Qi, X. Fan, J. C. Bui, D. V. Esposito, Int. J. H$_2$ Energy, 43(3), 1224-1238, 2018.

Collaborators in this area: West Group @ Columbia, Steingart Group @ Columbia, Shell, Kawashima Group @ Columbia, Qatar U., Texas A&M U. Qatar.

(Photo)electrocatalytic Materials

Metal Oxide-Encapsulated Nanoparticle Co-Catalysts[6]

Key idea: stabilize metal nanoparticles by encapsulation w/ ultrathin permeable oxide layer.

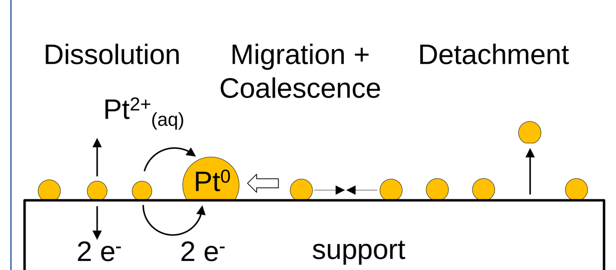

Mechanisms of Electrocatalyst degradation

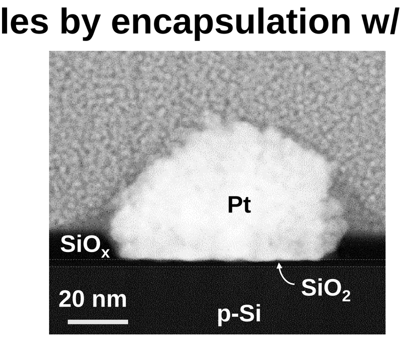

TEM image of SiO$_2$-coated Pt NP catalyst on native SiO$_2$/p-Si for light driven HER

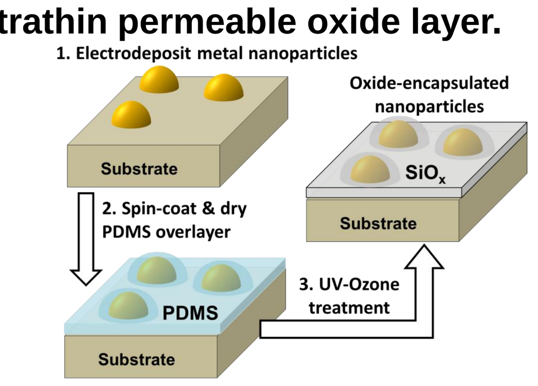

Room temperature UV-Ozone process for encapsulation of supported metal nanoparticles.

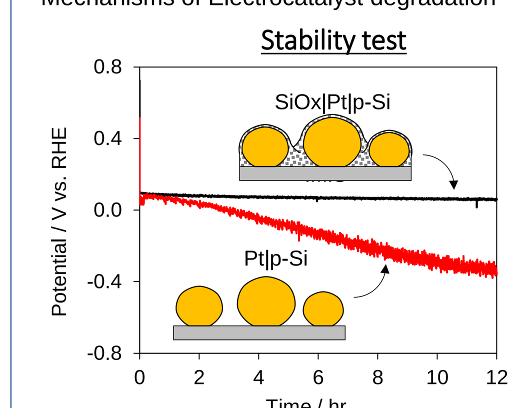

Operation at -10 mA cm^{-2} in 0.5 M H$_2$SO$_4$ for Pt/p-Si w/ and w/o a 10 nm SiO$_x$ overlayer.

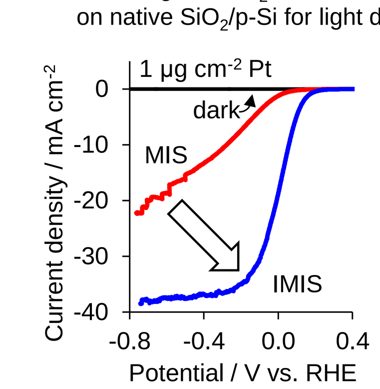

LSV in 0.5 M H$_2$SO$_4$ to evaluate improved H$_2$ evolution performance with SiO$_x$ overlayer

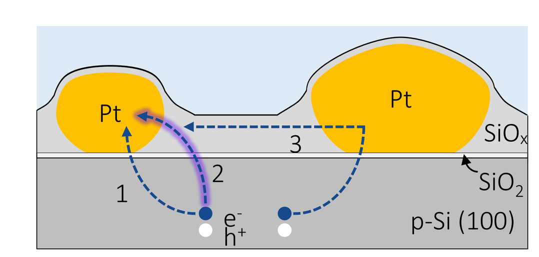

Possible mechanisms by which SiO$_x$ overlayer may decrease charge transfer resistance between p-Si and Pt nanoparticles.

Key Findings: Encapsulation of Pt nanoparticles with SiO$_x$ mitigates particle detachment/ agglomeration while enhancing charge transport b/w p-Si and metal nanoparticles.

1D Membrane Coated Electrocatalysts (MCECs)[7-10]

Key Idea: Use oxide overlayers to control reaction pathways by altering transport & kinetics.

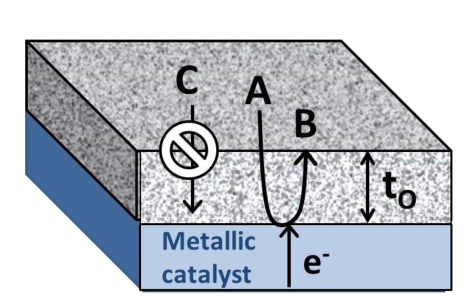

Well-defined oxide overlayer deposited on smooth metal thin film.[8]

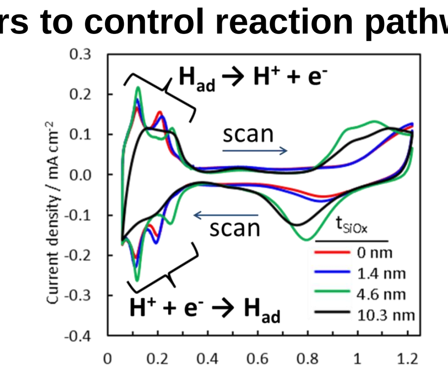

CV (100 mV s^{-1}) in 0.5 M H$_2$SO$_4$ for SiO$_x$|Pt electrodes.[9]

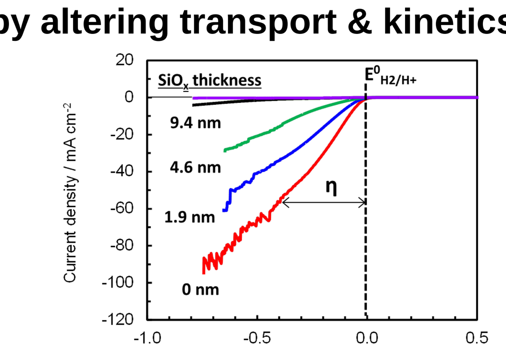

LSVs for planar SiO$_x$|Pt electrodes in 0.1 M H$_2$SO$_4$ at 20 mV s^{-1}.[7]

Key Findings: SiO$_x$ overlayers can alter reaction pathways by behaving like membranes to alter concentrations, and/or by altering reaction energetics at the SiO$_x$|Pt buried interface .

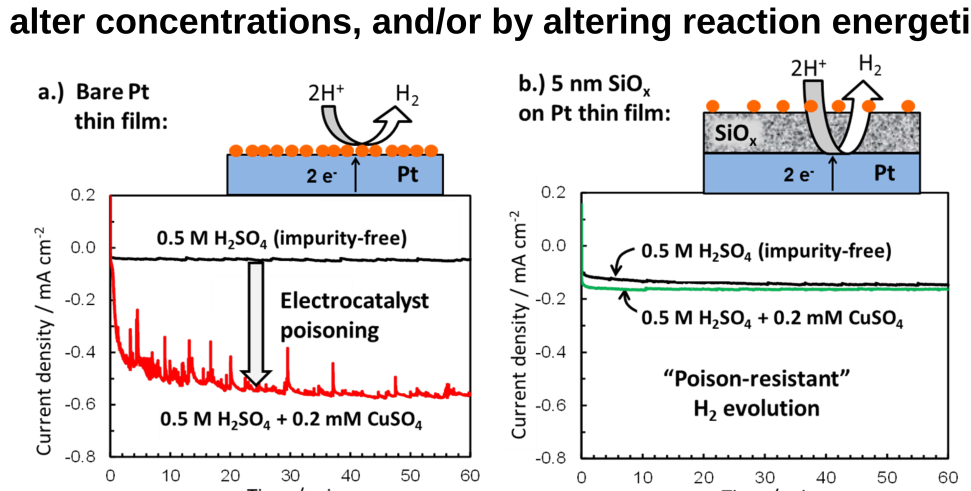

Constant current (5 mA cm^{-2}) chronopotentiometry curves in 0.5 M H$_2$SO$_4$ + 0.2 mM CuSO$_4$.[7]

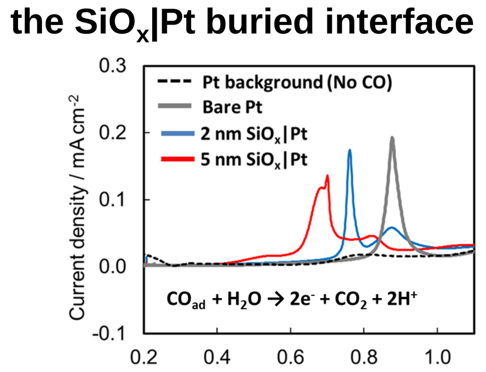

CO stripping voltammetry for SiO$_x$ electrodes in 0.5 M H$_2$SO$_4$ (25 mV s^{-1}).[10]

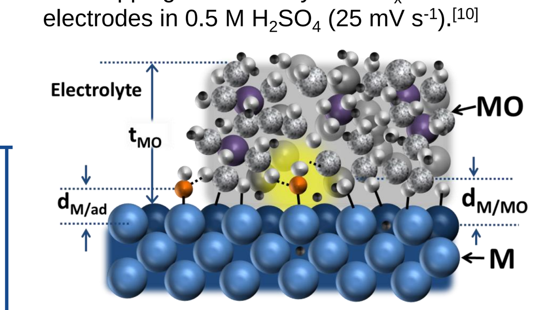

Molecular view of ultrathin metal oxide (MO) overlayer on metallic catalyst.[8]

Publications

[6] N. Y. Labrador, et al., Nano Letters, 16, 6452-6459, 2016.
[7] N. Y. Labrador, et al., ACS Catalysis, vol. 8, pp 1767–1778, 2018.
[8] D.V. Esposito, ACS Catalysis, vol. 8, pp 457–465, 2018.
[9] M. Beatty, H. Chen, et al., J. Mater. Chem. A., vol. 6, 2018
[10] N. Labrador, J. Robinson, ACS Catalysis, vol. 8, pp 11423-11434, 2018.

Collaborators in this area: Urban Group @ Columbia, Marbella Group @ Columbia, U. Michigan, UC Irvine, UC Davis, U. San Diego, LBNL.

In situ Analytical Tools

Our lab utilizes a suite of *in situ* analytical tools to interrogate the properties and performance of materials and devices with high spatial or temporal resolution.

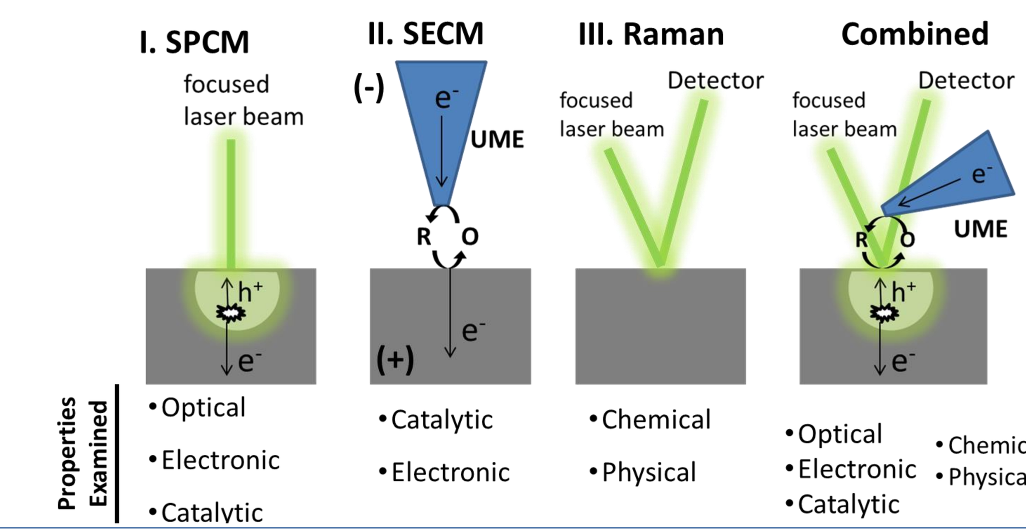

Scanning Photocurrent Microscopy (SPCM)[11,12]

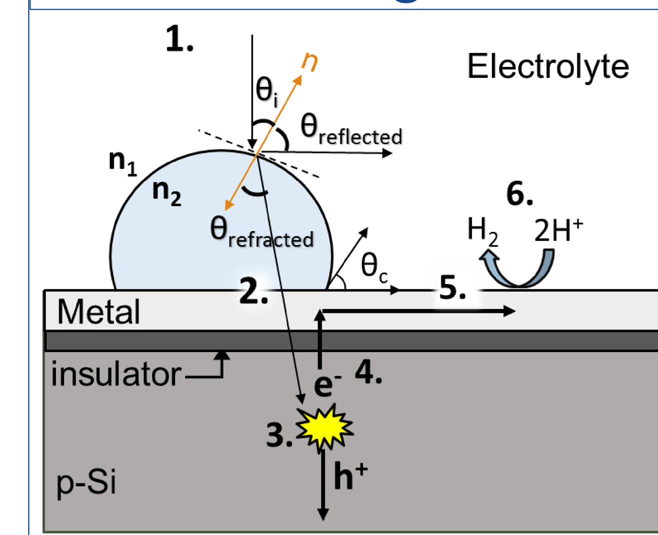

Metal-Insulator-Semiconductor (MIS) photoelectrode with a bubble attached to its surface.

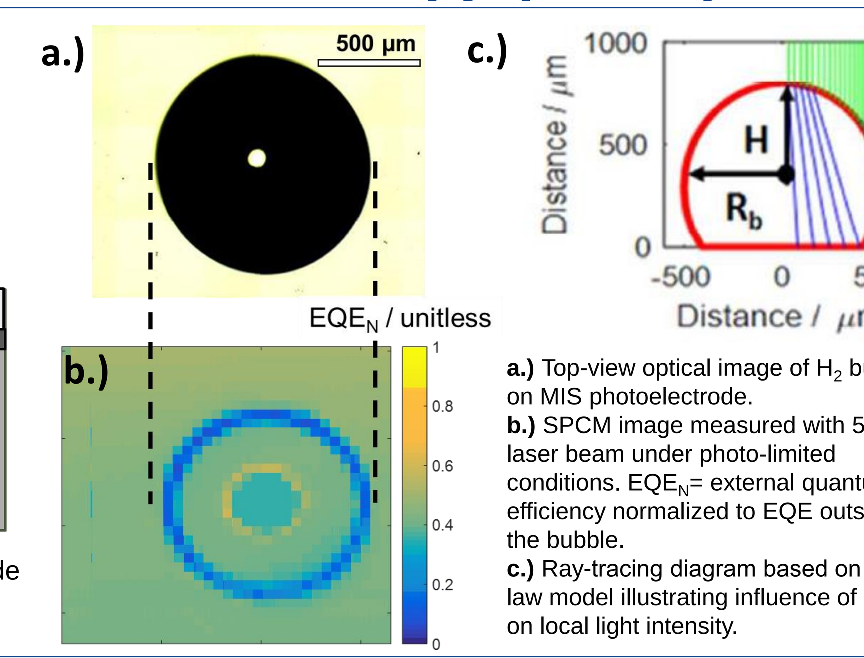

a.) Top-view optical image of H$_2$ bubble on MIS photoelectrode. **b.)** SPCM image measured with 532 nm laser beam under photo-limited conditions. EQE$_N$= external quantum efficiency normalized to EQE outside of the bubble. **c.)** Ray-tracing diagram based on Snell's law model illustrating influence of bubble on local light intensity.

Scanning Electrochemical Microscopy (SECM)[11,13]

Key idea: Use non-local probe geometries combined with compressed sensing (CS) signal analysis to increase areal scan rates and thereby enable nanoscale imaging over large areas.

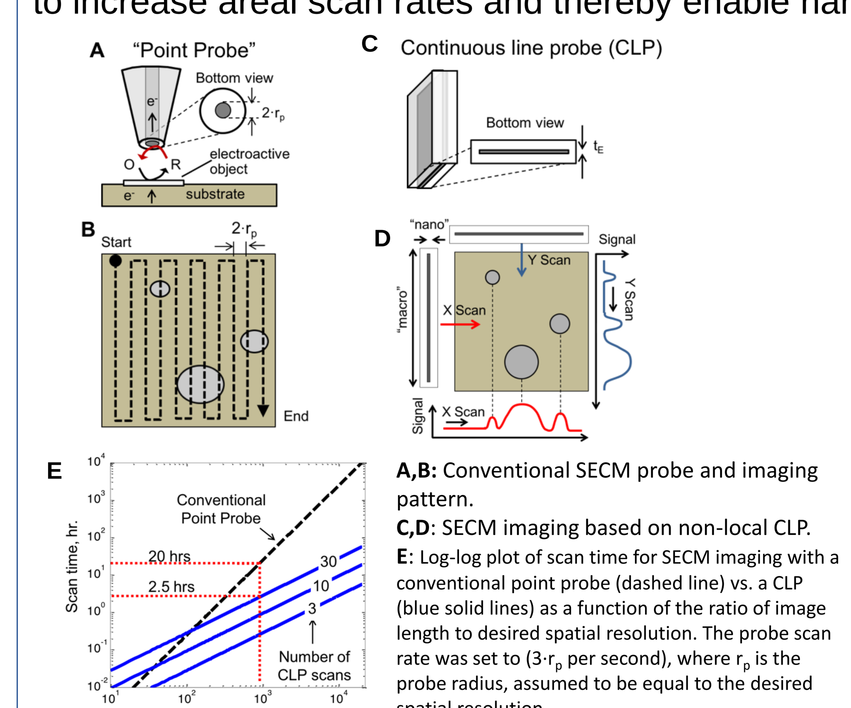

A,B: Conventional SECM probe and imaging pattern.
C,D: SECM imaging based on non-local CLP.
E: Log-log plot of scan time for SECM imaging with a conventional point probe (dashed line) vs. a CLP (blue solid lines) as a function of the ratio of image length to desired spatial resolution. The probe scan rate was set to (3·r$_p$ per second), where r$_p$ is the probe radius, assumed to be equal to the desired spatial resolution.

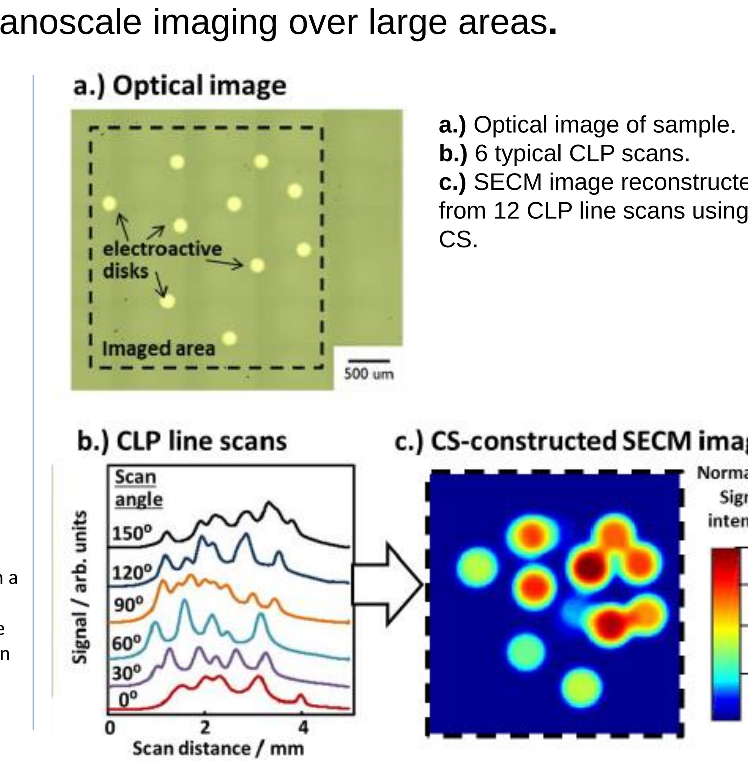

a.) Optical image of sample. **b.)** 6 typical CLP scans. **c.)** SECM image reconstructed from 12 CLP line scans using CS.

High Speed Video (HSV) Imaging[14]

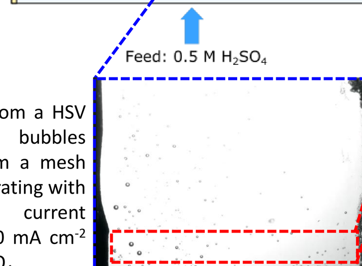

Still frame from a HSV showing H$_2$ bubbles evolving from a mesh cathode operating with an average current density of 50 mA cm^{-2} in 0.5 M H$_2$SO$_4$.

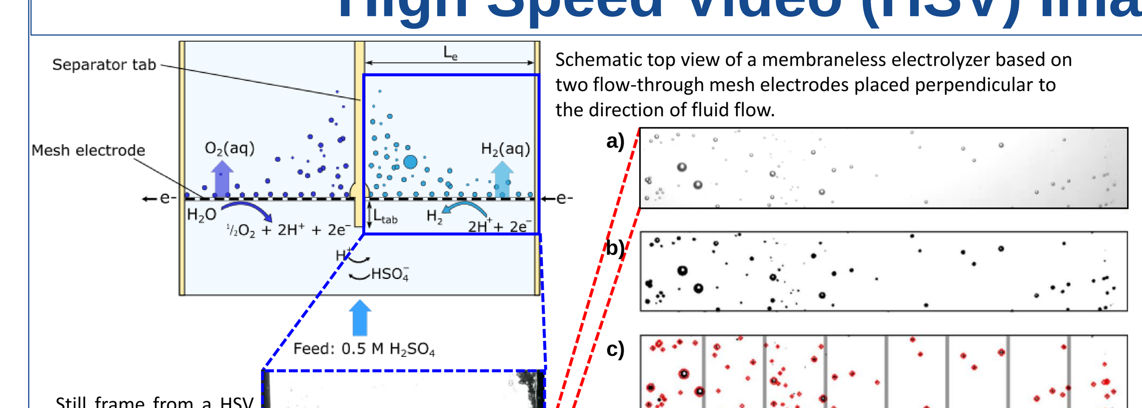

Schematic top view of a membraneless electrolyzer based on two flow-through mesh electrodes placed perpendicular to the direction of fluid flow.

a) The still frame is cropped to limit analysis to a narrow section. b) Conversion of the cropped still frame into a binary image to reduce background interference. c) The size and position of bubbles are determined using a circle detection algorithm. Discretizing the analysis area into equal control volume to estimate the local current density.

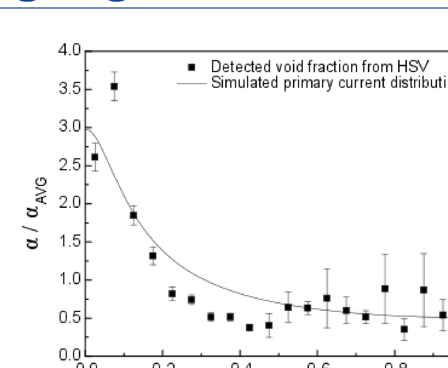

Comparison of the predicted current distribution to the local volume fraction along the length of the electrode, x/L$_e$.

Publications

[11] D. Esposito, J. Baxter, J. John, N. Lewis, T. Moffat, T. Ogitsu, G. O'Neill, T. Pham, A. Talin, J. Velazquez, B. Wood, Energy Env. Sci., 8(10), 2863-2885, 2015.
[12] A. E. Dorfi, A. C. West , D. V. Esposito, J. Phys. Chem. C., 121(48), 26587-26597, 2017.
[13] G. D. O'Neil, H. W. Kuo, D. N. Lomax, J. Wright, D. V. Esposito, Analytical Chemistry, 90(19), 11531-11537, 2018.
[14] J. T. Davis, D. E. Brown, X. Pang, D. V. Esposito, J. Electrochemical Society, 166(4), F312-F321, 2019.

Collaborators in this area: Wright Group in Electrical Engineering @ Columbia, West Group @ Columbia.